Astonish TF

Technical overview of Philips Time-of-Flight PET design and its clinical benefits

Amy E. Perkins, PhD, Senior Staff Physicist
Philips Healthcare – Nuclear Medicine, Cleveland, OH

Positron emission tomography (PET) continues to be on the forefront of molecular imaging. PET scanners have developed from research and brain instruments into clinical systems used routinely in clinical practice. In the past decade, PET imaging established itself as the gold standard for cancer staging and therapy followup. To a lesser extent, PET is also used clinically in cardiology (myocardial perfusion) and neurology (dementia).

The wide adoption of oncology applications of FDG PET imaging drove technology development towards (1) improvements in image quality and (2) integration with anatomical imaging (CT). PET image quality improvements were achieved by new detector design and architecture, commercial introduction and evolution of the Time-of-Flight PET, and patient motion management with respiratory and cardiac gated imaging. Recently, more emphasis has been placed on quantitative PET imaging for the purpose of lesion characterization and longitudinal data analysis.

In this paper, the PET technology choices Philips has made in designing Astonish TF will be discussed. Philips has an integrated technology approach to the entire imaging chain. Technical discussion will be illustrated with examples of some of the clinical applications that are enabled by this technology.

PHILIPS
sense and simplicity

Detector technology and data acquisition

There are several key choices in the design of a PET scanner which affect the specifications and clinical performance including crystal choice, electronics design, and image processing algorithms. The key technology components of the Astonish TF technology are described in this section.

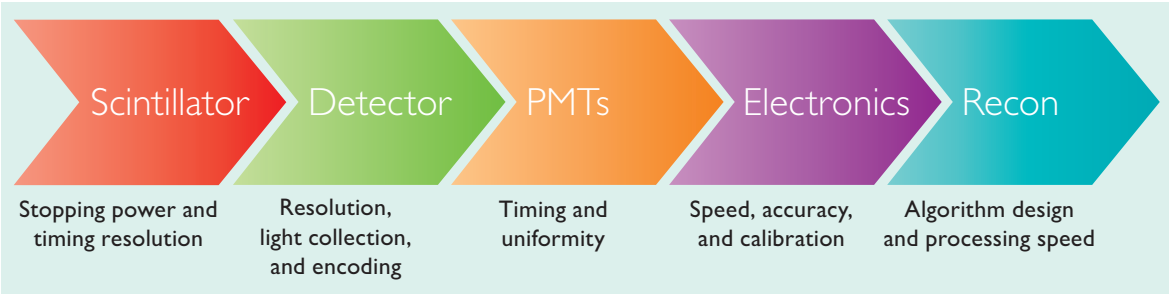

Figure 1 Astonish TF is an imaging technology that integrates all elements of the imaging chain into a state-of-the-art PET system. The choice of crystal material, detector and electronics design and image reconstruction architecture deliver industry-leading results in the system energy resolution, Time-of-Flight timing resolution, and reconstruction speed.

Crystal and detector design

One of the most fundamental elements of designing a high performing PET scanner is the choice of scintillator material. We have chosen to use LYSO as the scintillator because of its high light output, high attenuation coefficient, and fast timing performance. The very good timing resolution of the LYSO detectors enables Astonish TF PET imaging with a scanner timing resolution of 495 ps. Table 1 shows the key performance measures of scintillator materials that have been incorporated into PET instruments over the last several decades. For modern PET scanners, a short decay time and high light output is required for TOF imaging, and a high attenuation coefficient is needed for high sensitivity and good spatial resolution. LYSO possesses these characteristics. Astonish TF technology is comprised of pixilated LYSO crystals arranged in an Anger-logic detector design to achieve uniform light spread in the detector. The detector is shown in Figure 2.

Scintillator	Decay time (ns)	Attenuation coefficient (cm^{-1})	Light output (photons/MeV)
NaI(Tl)	230	0.35	41000
BGO	300	0.95	7000
GSO	60	0.70	10000
BaF_2	2	0.45	2000
LYSO, LSO	40	0.86	26000
$LaBr_3$	20	0.47	60000

Table 1 Anger-logic readout of LYSO crystals provides excellent TOF, uniform energy resolution performance, and good count-rate behavior.

Figure 2 The Astonish TF technology design. The 4 mm x 4 mm x 22 mm LYSO crystals are assembled in a 23 x 44 array and are coupled through a light guide (left) to a hexagonal arrangement of fast PMTs to create a detector module (middle). Multiple modules are assembled in the scanner (right).

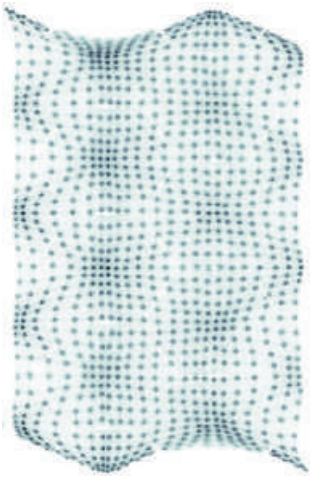

Figure 3 Crystal map for one detector module. Each dark spot corresponds to an individual LYSO crystal. Good pixel separation is observed with Astonish TF technology. resolution, and reconstruction speed.

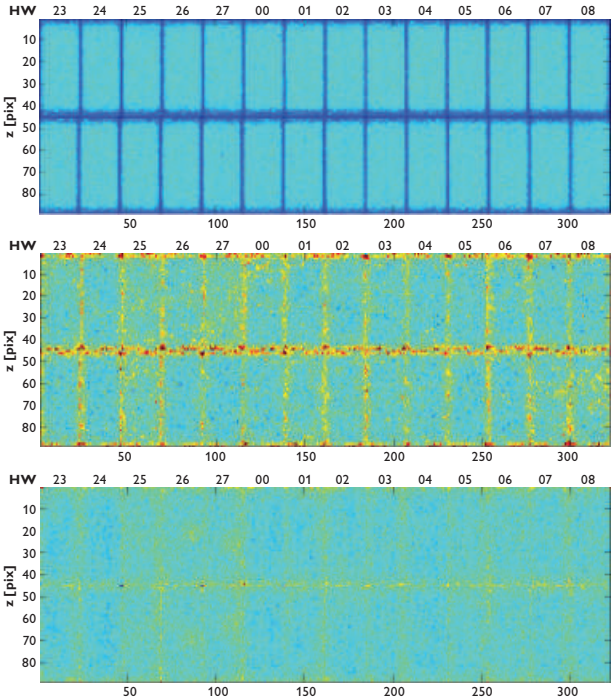

Figure 4 Plots of individual crystal counts (top), energy FWHM (middle), and timing FWHM (bottom) from a point of activity at the center of the scanner. Each point in the plots corresponds to different crystals arranged according to its position in the scanner: around the scanner (X position, left/right) and axially (Z position, up/down). To save space, half of the scanner is plotted on the top and the second half is plotted directly underneath. The individual 28 modules can be seen in these images. The energy (and timing) centroids for each crystal have been calibrated so that they are all aligned to the same values.

The count-rate capability of the large detector module is optimized by using small, 7-PMT clusters for both position and energy calculation.

The scintillation light from all of the crystals in Astonish TF technology are more uniformly collected in this large, continuous Anger-logic design [Surti 2000, Karp 2003, Kuhn 2004] than in the smaller block design [Casey 1986, Wong 1995, Cherry 1995], and this leads to good crystal separation (Figure 3) with more uniform energy and timing resolution across the crystals. This crystal map is linearized by assigning an actual scanner crystal X and Z position to each point in the map. The uniformity of the counts, energy FWHM, and timing FWHM of the individual crystals across the entire scanner are shown in Figure 4.

As a result of the good average scanner energy resolution (12%), tight energy windows (440-665 keV) lead to a reduction in the system scatter fraction (30% scatter fraction as measured by NEMA NU2-2007). The fast timing properties, high light output, and high stopping power of LYSO combined with this technology design lead to a high-sensitivity scanner with good counting rate capability and very good spatial, energy, and timing resolutions [Surti 2007].

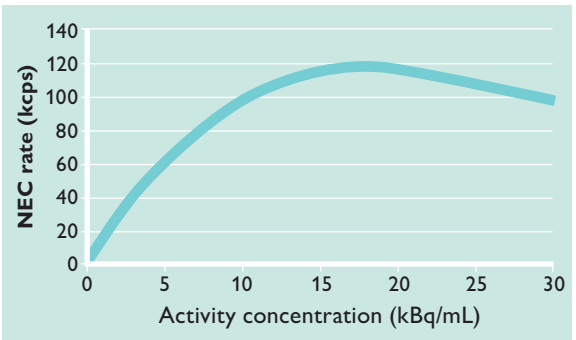

Figure 5 NEC rate versus activity concentration for a NEMA countloss cylindrical 20 cm diameter phantom.

As a result of the high throughput electronics, Astonish TF maintains high Noise Equivalent Counts (NEC) values at high scanner rates, or injected activity values, as seen in Figure 5. This is particularly important for high injection dose clinical scans, such as cardiac imaging. The decrease in NEC at very high activity concentrations is due to high randoms rates which affects all PET scanners.

3D imaging provides higher sensitivity

The sensitivity of PET scanners has become a very important criteria in clinical applications in which high quality images are required in short acquisition scans and with low injected doses to the patients. Historically, due to poor energy resolution, PET scanners operated in 2D mode using absorbing septa to limit the scattered events. This design limited the potential system sensitivity by as much as 80%. Philips recognized this limitation and was one of the first to fully commit to 3D imaging commercially. Astonish TF technology operates in a fully 3D mode in order to increase sensitivity. High sensitivity imaging is of particular importance to produce good image quality for large patients. In addition, Astonish TF technology offers TOF PET imaging which provides additional benefits for large patients.

PET scanners operating in 2D mode use an absorbing septa to limit most of the scattered events. However, this reduces the sensitivity of the scanner. Energy resolution is not as important when operating a scanner in 2D mode since there is little scatter. The count-rate is kept low and therefore the deadtime is low, so the demands on the count-rate capability of the system are modest.

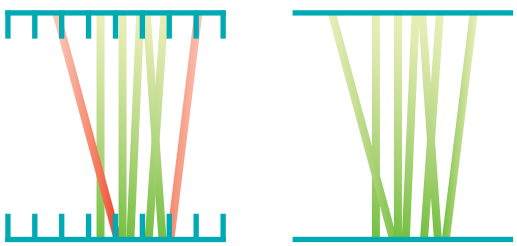

Figure 6 In 2D mode (left) only 'in-plane' lines of response (LORs) are accepted. In 3D (right) LORs at all angles are accepted and the sensitivity is increased. 3D imaging leverages the advantages of fast, modern crystals with excellent light output and energy resolution.

The design considerations for fully 3D PET scanners are quite different. The removal of the septa increases the sensitivity. In this case the count-rates are much higher and the deadtime and randoms can become much more of a factor. The count-rate capability is more of a concern for Rb-82 cardiac studies on 3D scanners with high injected doses. Scattered events are much higher in 3D and good energy resolution is required to reduce the scatter. The scattered and random events can be kept low with a modern detector design with good energy resolution by raising the lower energy threshold.

TOF imaging

In PET imaging, coincident gamma rays are emitted from the annihilation of a positron-labeled radiopharmaceutical injected into the patient. The gamma rays are detected by the PET scanner and tomographic images are created through traditional filtered back-projection, or through an iterative series of back- and forward-projection steps (Figure 7). In a conventional system there is no information about where along the line of response (LOR) the annihilation event occurred, and the image reconstruction algorithm assumes a uniform probability along the LOR for the location of the event. With Astonish TF technology, the system measures the TOF difference between the arrival times of each coincident pair of annihilation photons with precision that the estimated position of the event can be localized along the LOR with a Gaussian distribution with a full width at half maximum (FWHM) $\Delta x = c\Delta t/2$, where c is the speed of light and Δt is the system timing resolution.

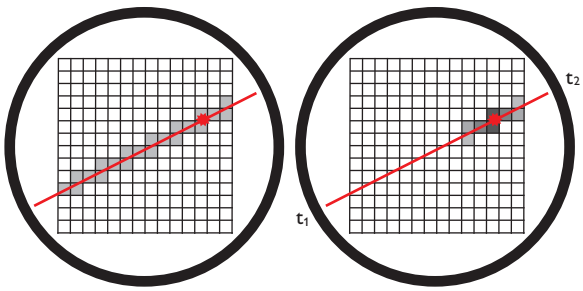

Figure 7 In conventional PET (left) there is no localization along the line of response. Astonish TF technology (right) is able to pinpoint the annihilation event more precisely along the LOR.

The ratio of the patient size (D) to the positional uncertainty (Δx) is representative of the noise reduction, or the sensitivity gain, with TOF in a uniform cylinder without considering reconstruction effects and assuming a uniform distribution of activity [Budinger 1983, Tomatami 1981].

TOF sensitivity gain ~ $D / \Delta x$

This benefit in TOF increases as the PET system timing resolution improves but, perhaps more importantly, TOF provides more benefit in the case of heavy patients whose PET images are often of lesser quality in conventional PET, due to increased attenuation and scatter.

Following early TOF scanners in the 1980s, Philips launched the first commercially available TOF system with its GEMINI TF System in 2006 featuring 650 ps timing resolution. In the last five years Philips continued to improve this technology, and Astonish TF technology represents recent advancements including industry leading 495 ps timing resolution.

Philips product	Timing resolution	Positional uncertainty
Gemini TF	650 ps	9.8 cm
Gemini TF Gen2	575 ps	8.6 cm
Astonish TF	495 ps	7.4 cm

Table 2

Reconstruction

The choice of reconstruction methodology is extremely important for system performance. Astonish TF technology, by means of list mode data acquisition, allows Philips to select the best-in-class reconstruction algorithm without compromise. Astonish TF delivers fast reconstruction speed and increases the clinical throughput without compromising the image quality, such as spatial resolution. Image quality and quantitative accuracy are very important in today's PET/CT clinic and this section discusses the choices made in the reconstruction design of Astonish TF technology for excellent performance.

Full data fidelity and flexibility is maintained using list mode TOF reconstruction

An image is created from the acquired line of response (LOR) data with the use of a reconstruction algorithm. Astonish TF utilizes list mode TOF reconstruction, maintaining full data fidelity and flexibility through the reconstruction process. The TOF information is included as a TOF kernel width in the relaxed TOF list mode ordered subsets expectation maximization (OSEM) algorithm with chronologically ordered subsets [Popescu 2004, Wang 2006]. The reconstruction is fully 3D and provides a more accurate matching of scanner geometry and reconstruction, eliminating artifacts and limitations specific to reconstruction that is not fully 3D. The attenuation, scatter and randoms are modeled in the system matrix, while the detector normalization, isotope decay, system dead-time and crystal timing corrections are pre-corrected for each list mode event. Scatter is estimated from a TOF-extended single scatter simulation (TOF-SSS) [Watson 2007, Werner 2006]. The implementation details of the Astonish TF reconstruction can be found in [Wang 2006].

Conventional reconstruction in PET imaging involves an LOR preprocessing step where the raw LOR data are rebinned and interpolated to evenly spaced sinogram data, as shown in Figure 8. The sinogram-mode reconstruction methods often combine certain nearby LORs into the same sinogram bin and thereby degrade the image resolution, especially away from the center of the field-of-view (FOV). The LOR-based and list mode reconstruction eliminates this interpolation step and thus gives rise to better spatial resolution and image quality [Kadrmas 2004]. In Astonish TF technology, this approach is combined with an overlapping spherically symmetric volume (blob) basis function that leads not only to substantial suppression of the image noise but also to preservation of the resolution compared to conventional cubic voxels [Matej 1996b]. This blob approach allows Philips scanners to achieve better contrast-to-noise performance over voxel reconstruction [Hu 2007].

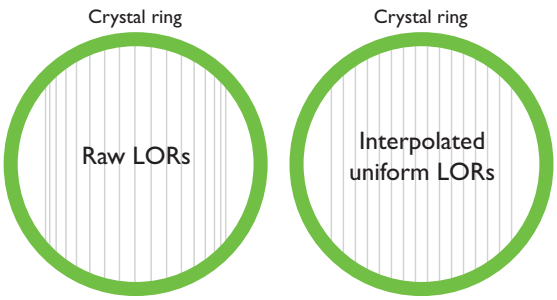

Figure 8 Raw LORs (left) versus interpolated uniform LORs (right).

An improvement in image quality when the data are reconstructed directly from the unprocessed list mode data rather than various rebinning methods has been demonstrated [Liu 2001]. TOF list mode reconstruction produces more uniform spatial resolution and better contrast-noise trade-off than single-slice rebinning (SSRB) [Vandenberghe 2006]. Fully 3D reconstruction has been shown to be superior to discrete data rebinning techniques [Defrise 2008].

As an example of the improvement with list mode reconstruction, the data from a rectal carcinoma patient with metastases in mesentery and bilateral iliac chains were reconstructed with 3 different algorithms (Figure 9). The lesions are most clearly detected and the image quality is improved when all the data are preserved (i.e., the list mode reconstruction). The data size for the RAMLA [Matej 1996a] sinogram-based reconstruction and the LOR-based reconstruction with phi combining is 8% and 50%, respectively, of the list mode data size

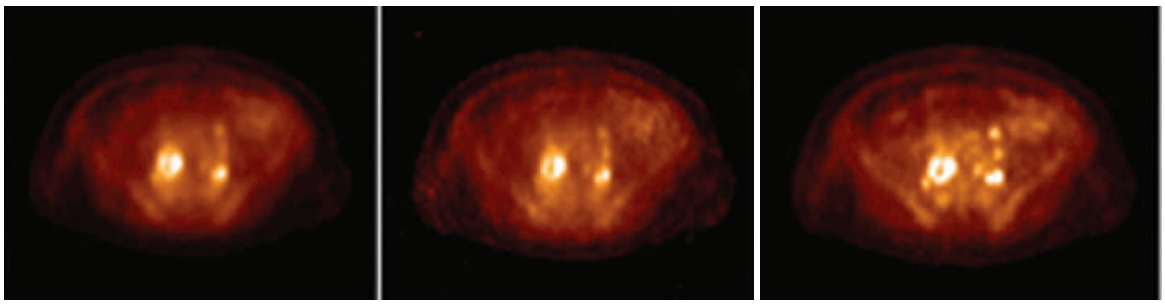

Figure 9 The same data were reconstructed with 3 different reconstruction algorithms: left = 3D RAMLA sinogram-based (data size = 15 MB), middle = LOR-RAMLA with phi mashing (data size = 99 MB), and right = listmode (data size = 198 MB). Images courtesy of Prof. Joel Karp at the University of Pennsylvania.

in this particular example. The number of counts was maintained in this example, only the data size changed due to sinogram histogramming and phi combining.

The arrival time difference of the coincident pair of annihilation photons is preserved in list mode, as opposed to methods which rebin the data according to timing bins. This TOF information is directly stored in the list mode file to fully take advantage of the benefits of TOF imaging and reconstruction.

TOF-PET imaging has been shown to yield improved lesion detection and more accurate quantitation due to faster and more uniform convergence of lesion uptake at a fixed activity level [Surti 2007, Karp 2008, Surti 2009]. The increase in signal-to-noise ratio (SNR) may be used to improve image quality, reduce the dose to the patient, or reduce the scan time to improve patient comfort [Kadrmas 2009]. Recent work by El Fakhri and Surti [El Fakhri 2011, Surti 2011] has quantified the improvement of detectability of lung and liver lesions with TOF-PET in clinical whole-body 18F-FDG oncology studies. TOF-PET imaging has also been shown to be more robust in the presence of inconsistent data [Conti 2011].

Fast reconstruction speed

Image reconstruction from PET procedures is a complex, data-intensive, and computationally expensive task. The latest achievements in high-performance computing processors from Intel, optimized software, and advanced software programming methodologies are used with Astonish TF to enable faster completion of image reconstruction – in as little as a few minutes after the completion of data acquisition – benefiting patients and clinicians alike. These advances in PET image reconstruction allow radiologists and department managers to improve patient care, reduce the time to diagnosis, and boost department productivity.

Servers in a PET system create images by processing large amounts of data using software-based reconstruction algorithms. While this is a simplified view of the reconstruction system, it focuses on the need for an optimal balance of fast hardware, efficient and fast algorithms with an appropriate data model, and optimized software architecture and code.

In a specific example of a high throughput day-long clinical workflow performance analysis, the new Astonish TF technology reconstructs entire images as much as 5 times faster on average than existing Generation 2 systems, and as much as 20 times faster than Generation 1 systems. Figure 10 shows the behavior of the different generations of the Philips reconstruction during the afternoon workflow at a busy clinical PET center. PET/CT scans begin in the morning (not shown in Figure 10) and the most challenging part of the day is during the afternoon and evening hours after several scans have already been performed. Generation 1 cannot keep pace with the heavy clinical workflow and a backlog of longer reconstruction time forms in the afternoon. Because of longer reconstruction times, several reconstructions run simultaneously and compete for the same reconstruction resources (CPU, memory, etc.). This is exacerbated when retrospective reconstructions are added to the heavy clinical schedule. Both patient throughput and system reliability are impacted. The faster reconstruction of Generation 2 reduces the overlap of different reconstructions. The further improvement in reconstruction performance seen in the latest release of products (GEMINI TF 16, 64, and Big Bore, and TruFlight Select) means PET images can be available to clinicians before the next procedure begins.

TOF cardiac Rb-82 imaging

Recently, Philips introduced new reconstruction hardware and software on many of the new PET/CT systems.

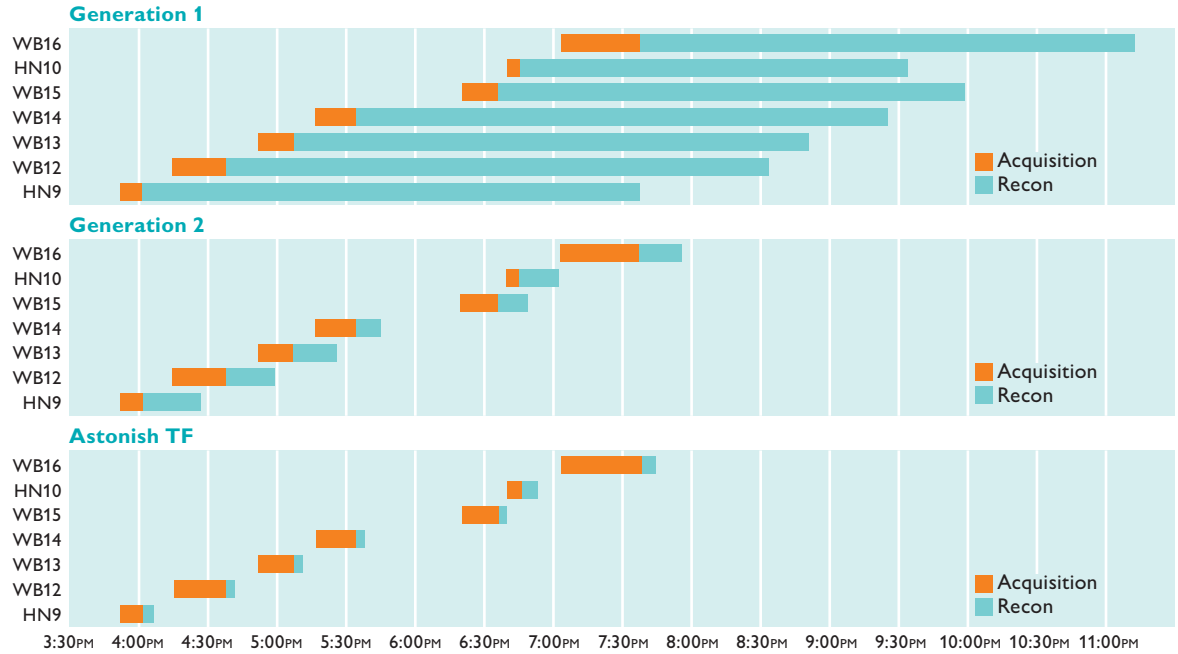

Figure 10 Acquisition and reconstruction times for seven procedures performed in the afternoon after a full patient schedule in the morning (not shown): Concurrent acquisition and reconstruction, plus overlapping reconstruction on a Generation 1 system (top), Improved performance with only concurrent acquisition and reconstruction on a Generation 2 system (middle), Reconstruction completed in minutes, before next acquisition with Astonish TF technology (bottom). WB = whole-body scan, HN = head and neck scan.

The benefits of this introduction are discussed in this section of the white paper. Myocardial perfusion imaging with Rb-82 poses unique challenges due to its rapid decay resulting in low count density, having the potential to affect image quality. Astonish TF's faster reconstruction speed allows the use TOF reconstruction for cardiac applications. The addition of TOF imaging has been shown to improve cardiac Rb-82 imaging [Tipnis 2008]. In this particular study, images reconstructed with the TOF method showed an average increase of 25% in the contrast to noise (CNR) in the left ventricular wall and the cavity as compared to those reconstructed with non-TOF reconstruction. The higher CNR is maintained in the TOF images even with low-count density acquisitions as shown in Figure 11. This could potentially allow lower doses to be used.

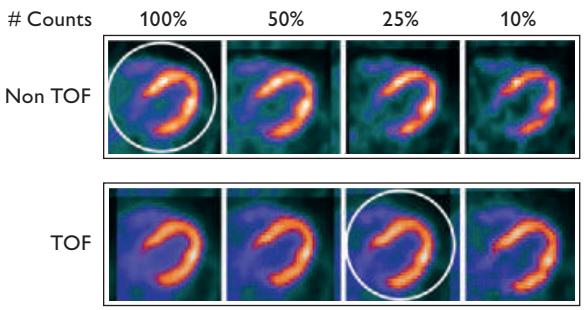

Figure 11 Effect of TOF and number of counts for a cardiac reconstruction. TOF reconstruction with 25% of counts is equivalent to non-TOF with all counts. [Tipnis 2008]

Point spread function (PSF) correction

The finite spatial resolution from any scanner demonstrates the limitation in the response of the system. Small objects and sharp delineations of contrast can become blurred. By modeling the point spread function (PSF) of the system, Astonish TF provides a more quantitatively accurate representation of the activity distribution without the addition of long processing times. The PSF correction approach provides improved image quality and accuracy by employing a more accurate representation of imaging physics.

The PSF describes the response of an imaging system to a point source. It is the spatial domain version of the modulation transfer function. The degree of spreading (blurring) of a point object is a measure of the quality of an imaging system. The image reconstructed from an imaging system can be expressed as the convolution of the true image and the PSF of the system, as illustrated on the left side of Figure 12. Astonish TF includes a post-reconstruction resolution recovery method using maximum-likelihood expectation maximization (ML-EM) de-convolution. The ML-EM de-convolution algorithm is used with the modeled system PSF to improve clinical PET image quality as illustrated in the right side of Figure 12.

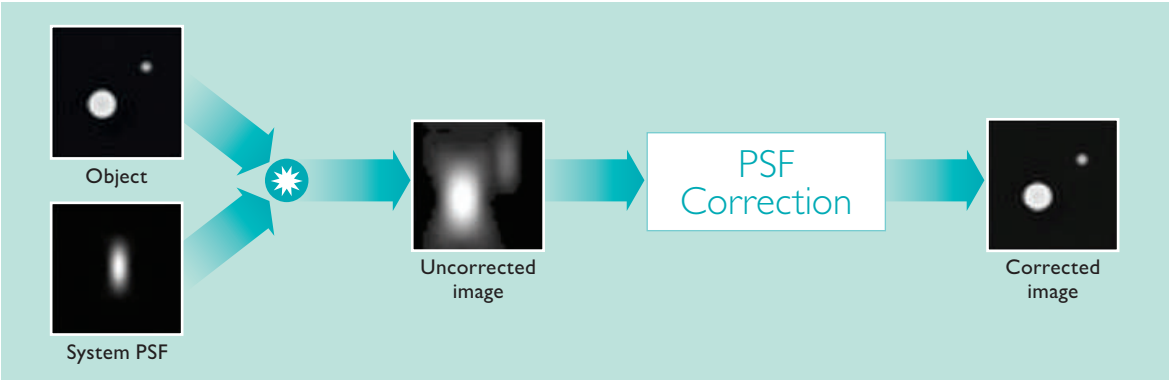

Figure 12 The PSF of the system blurs the object to be imaged and Astonish TF uses PSF correction to improve the image quality of the resulting image.

The ML-EM de-convolution algorithm [Richardson 1972, Lucy 1974, Biggs 1997] is an iterative technique used in the restoration of images in the presence of Poisson noise in medical imaging and also in astronomy. It attempts to maximize the likelihood of the restored image by using the EM algorithm. The algorithm requires the PSF of the system which is obtained by measuring point sources at different locations within the scanner field of view. The Astonish TF approach models the true, spatially varying PSF of the scanner. The advantage of ML-EM deconvolution over Fourier methods such as Wiener filtering is better modeling of the image blurring process and the assumption of a Poisson model for the image.

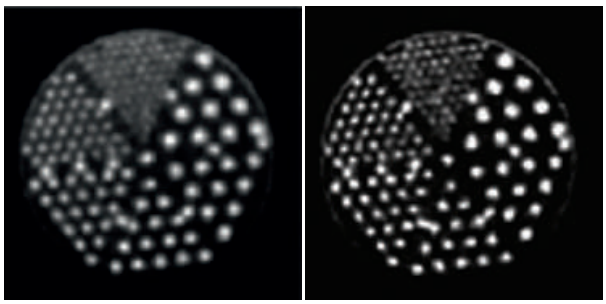

Figure 13 The images of the Jaszczak phantom without PSF correction (left) and with PSF correction (right).

The partial volume effect (PVE) is a major source of bias in clinical PET imaging [Cloquet 2010]. The causes of PVE include LOR position approximations, finite crystal size, positron range, acollinearity, parallax, and intercrystal scatter. The PVE can be reduced by accounting for the PSF of the PET scanner. As PSF represents the blurring effect of the PET imaging, by properly measuring and modeling the system PSF, PET image quality can be improved by a deblurring process using the PSF information. Image quality can be improved by using PSF information as it improves the modeling accuracy of the imaging process such that image resolution and contrast can be recovered and enhanced with moderate noise propagation [Snyder 1985].

The image quality is improved with Astonish TF through the use of PSF as demonstrated by the images of the Jaszczak phantom (Figure 13). Overall, the hot rods have higher contrast in the PSF image. The 4.8 mm diameter rods in the smallest sector are more easily distinguished in the image with PSF.

The spatial resolution and contrast improvements demonstrated with phantoms, translate to noticeable improvements in clinical data. Both TOF and PSF have been implemented for brain studies. Figure 14 shows a typical clinical brain study with approximately 250 Mcnts. The left column shows the transverse and coronal slices of the non-TOF image and the right column are the corresponding slices for the TOF image with PSF.

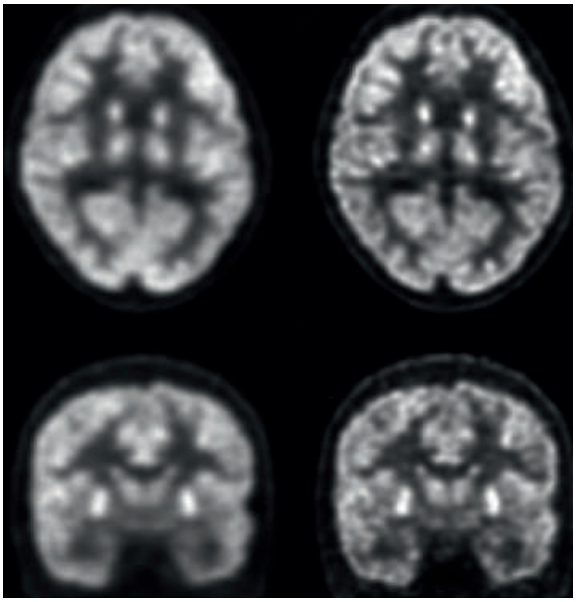

Figure 14 Clinical brain images using LOR RAMLA without TOF and no PSF correction (left) and with listmode TOF+PSF correction (right). The top row shows the transverse slices and the bottom row displays the coronal slices.
Patient data courtesy of University Hospital, Cleveland, USA.

Spatial resolution less than 2 mm

Combining the approaches described in the preceding section, Astonish TF has demonstrated the ability to recover resolution to less than 2 mm. As demonstrated with 1 mm point sources, Astonish TF has the ability to reconstruct the sources to measure less than 2 mm in the image. Figure 16 shows that the resolution improves isotropically from the center of the image field.

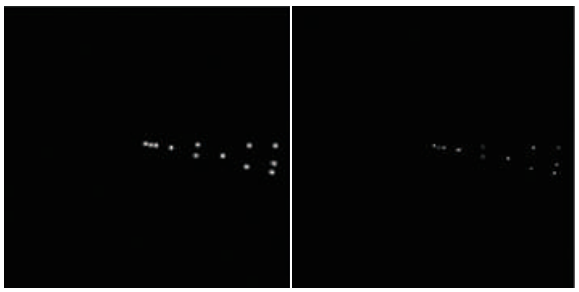

Figure 16 Point Source (1 mm) images with 4 mm voxel reconstruction without PSF correction (left) and 2 mm voxel reconstruction with PSF correction (right).

2 mm voxel whole-body reconstruction benefits

In addition to the benefits of TOF and PSF, Astonish TF technology offers new reconstruction protocols with 2 mm image voxels. Image quality improvements in whole body imaging are demonstrated in Figure 15 in which the same data were reconstructed with 4 mm voxels and 2 mm voxels + PSF.

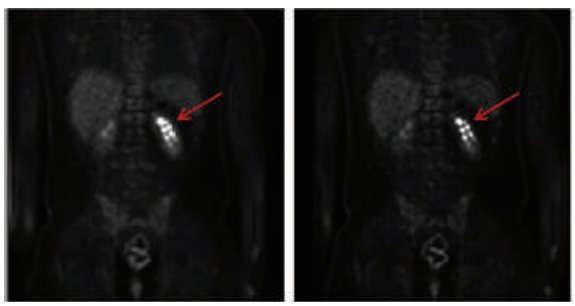

Figure 15 Clinical images with 4 mm voxels (left) and 2 mm voxels + PSF correction (right).
Patient data courtesy of University Hospital, Cleveland, USA.

4D PET

A significant source of image degradation in both CT and PET is represented by organ movements, mainly due to cardiac and respiratory motion, affecting image quality and quantitative accuracy for diagnostic purposes as well as the ability to define accurate target volumes in radiation oncology [Bettinardi 2010]. In diagnostic PET/CT studies respiratory gating is used to better localize abnormalities near the borders between the lung and liver, as well as for the detection of very small lesions that are "blurred" into the background activity by respiratory motion. The aim of 4D-PET/CT techniques is, in fact, to produce "motion free" and well matched PET and CT images corresponding to specific phases of the patient's respiratory cycle. 4D PET/CT techniques might have a great impact on clinical diagnostic applications, where the goal is the detection and the accurate metabolic characterization of lesions affected by respiratory movements and radiation therapy, where the goal is to assess, the true volume of the lesion and its real motion, to obtain an accurate target delineation and, in general, a more accurate and personalized definition of the treatment plan [Bettinardi 2010].

By increasing the effective sensitivity with 3D TOF imaging, Astonish TF provides good quality gated imaging. The PET/CT Pulmonary Toolkit application allows visualization of respiratory correlated data improving clinical confidence in data interpretation. The pulmonary gating application helps assure high-quality imaging of respiratory motion.

Respiratory gating

Respiratory gating has been shown to improve the detection of small pulmonary nodules on PET/CT [Bernard 2007]. In this study, a significant reduction in lung nodule blurring was noted for lesions located within the lung parenchyma, with maximal standardized uptake value (SUVmax) increases ranging from 23–123% in small lesions. Smaller lesions were visually more conspicuous and striking SUVmax increases were noted in small lesions. In some cases, small lesions clearly seen on CT but negative on conventional PET images could be clearly resolved on the respiratory gated PET images. Shape distortion on CT and PET/CT mismatch were also corrected with the use of respiratory synchronized CT data. Figure 17 shows the images with and without respiratory gating. In this patient, the respiratory gating increases the SUVmax of the lung lesion from 1.55 to 3.48.

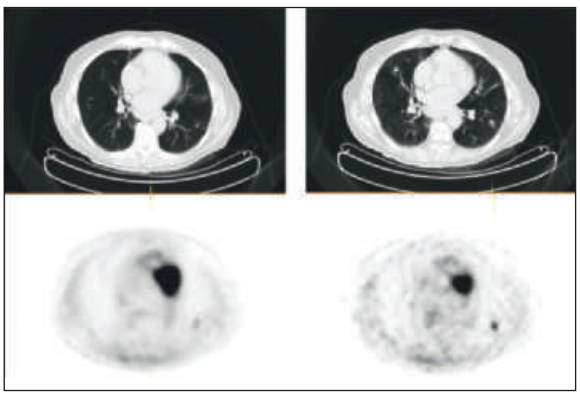

Figure 17 The CT (top) and PET (bottom) images without respiratory gating (left) and with respiratory gating (right). The maxSUV for the lung nodule increases from 1.55 to 3.48 with the addition of respiratory gating. [Bernard 2007]

Clinical studies

This section highlights the clinical benefits of TOF-PET imaging as demonstrated by [Karp 2008]. TOF was shown to lead to a better contrast recovery coefficient (CRC) versus noise trade-off in both phantoms and patients. TOF reconstruction results in a higher contrast recovery at matched noise with faster and more uniform convergence, and the benefit is even greater for larger patients. Lesions in patient studies are seen more clearly and with higher uptake at comparable noise for TOF than with non-TOF.

Figure 18 shows transverse images for 2 heavy patients: (top) with colon cancer (weight = 119 kg, BMI = 46.5) and (bottom) with abdominal cancer (115 kg, BMI = 38). In both cases, the images reconstructed with TOF (right) have improved structural detail. The first example indicates uptake in a lesion, correlated with CT, which is difficult to see in the non-TOF image.

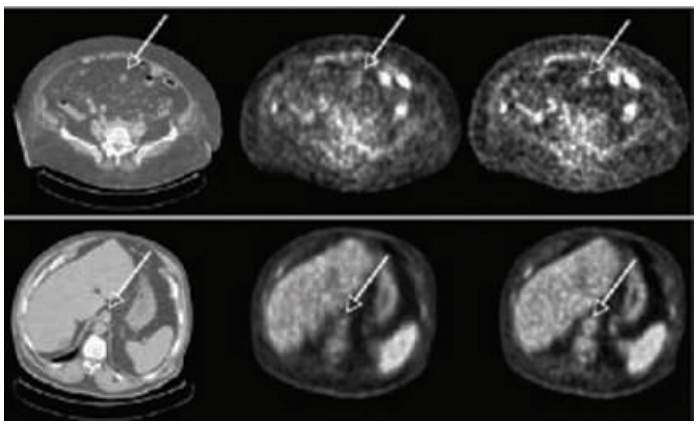

Figure 18 Representative transverse sections of 2 different patients: low dose CT (left), non-TOF (middle), and TOF (right). (Top) Patient 1 with colon cancer (119 kg, BMI = 46.5) shows a lesion in abdomen seen in CT much more clearly in TOF image than in non- TOF image. (Bottom) Patient 2 with abdominal cancer (115 kg, BMI = 38) shows structure in the aorta seen in CT much more clearly in TOF image than in non-TOF image. [Karp 2008]

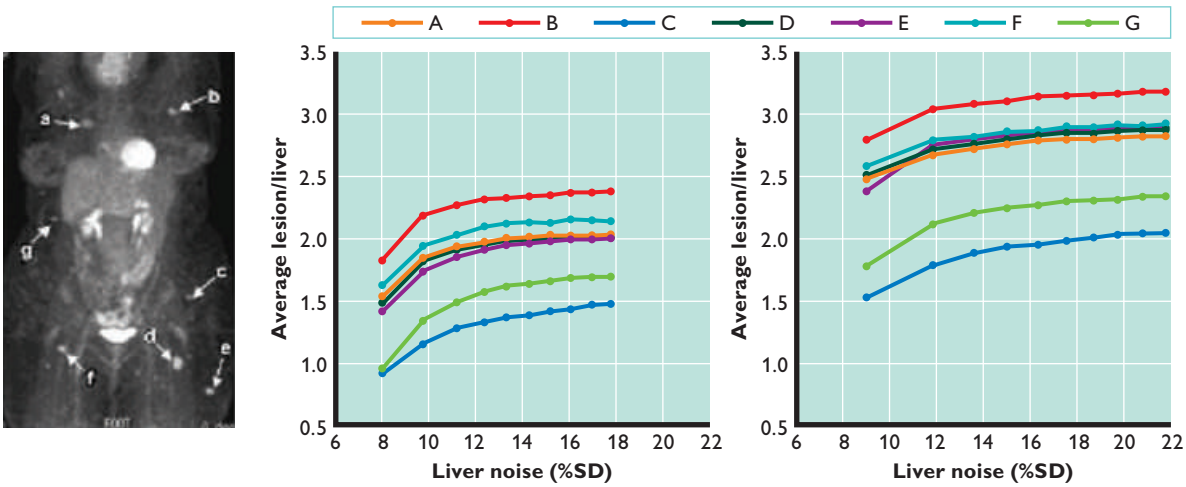

Figure 19 Patient with non-Hodgkin's lymphoma (140 kg, BMI = 46). (Left) Anterior projection image after 10 iterations of TOF MLEM reconstruction is shown. Letters (a–g) denote lesions that were used in the L/B ratio analysis. L/B ratio is plotted vs. noise in liver ROI for 1–10 iterations for each lesion for non-TOF (middle) and TOF (right) reconstructions. [Karp 2008]

Figure 19 shows the improved contrast recovery achieved with TOF information in a third patient. Figure 19 (left) shows an anterior projection image where the letters (a–g) denote the lesions used in the lesion-to-background (L/B) ratio analysis. Figure 19 (middle and right) shows plots of the L/B ratio as a function of noise in the liver ROI for each lesion without (middle) and with (right) TOF. The TOF gain was calculated as the ratio of L/B ratio with TOF to that without TOF. The L/B ratio curves with TOF have reached or are very close to convergence by 10 iterations. In fact, the L/B ratio with TOF is within 95% of the 10-iteration value after 4 iterations. The results suggest that convergence with TOF is more spatially invariant, as noted in other studies [Vandenberghe 2006, Perkins 2010]. In addition, higher TOF gain was correlated with increasing patient size, which has been supported by a larger patient study of 30 patients [Perkins 2007].

TOF allows one to image for shorter times and still achieve good image quality. With or without TOF, image noise increases for shorter scans because fewer events are detected; however, TOF reconstruction leads to improved structural detail, so images with fewer counts may still have satisfactory image quality. This implies that TOF can be beneficial in situations where few counts are collected – for example, dynamic imaging, respiratory gating, and imaging with nonpure positron-emitters.

The Philips Astonish TF provides a platform for continuous clinical improvement with further improvements in the timing resolution.

Conclusions

Astonish TF provides excellent PET/CT image quality through Philips careful detector design choices which result in a high-sensitivity scanner with excellent counting rate capability, good scatter rejection, and very good spatial, energy, and timing resolutions. Astonish TF has an excellent timing resolution of 495 ps, further enhancing the benefits of TOF. The Astonish TF platform provides continuous improvement with further improvements in the timing resolution. By increasing the effective sensitivity with 3D TOF imaging, Astonish TF provides good quality gated imaging.

Excellent image quality is achieved with Philips reconstruction implementation. Astonish TF reconstruction technology has been shown to reconstruct images as much as five times faster on average than existing Generation 2 systems. PSF has been implemented in Astonish TF and the resulting images are sharper and have higher contrast. TOF imaging has been shown to produce excellent quality clinical oncology images. Lesion detection is improved and with higher uptake at comparable noise for TOF than with non-TOF, and the benefit may be more pronounced in large patients.

References

Bernard F, Turcotte E, Scheuermann J, Saffer J, Karp J, and Divgi C. Respiratory synchronization to improve the detection of small pulmonary nodules on PET/CT. Journal of Nuclear Medicine. 2007, Abstract Book Supplement 48:123.

Bettinardi V, Picchio M, Di Muzio N, Gianolli L, Gilardi MC, and Messa C. Detection and compensation of organ/lesion motion using 4D-PET/CT respiratory gated acquisition techniques. Radiotherapy and Oncology 2010 96:311–316.

Biggs DSC and Andrews M. Acceleration of iterative image restoration algorithms. Applied Optics 1997 36:1766–1775.

Budinger TF. Time of flight positron emission tomography: status relative to conventional PET. Journal of Nuclear Medicine 1983 24:73–78.

Casey ME and Nutt R. A multicrystal two dimensional BGO detector system for positron emission tomography. IEEE Transactions on Nuclear Science 1986 NS-33:460–465.

Cherry SR, Tornai MP, Levin CS, Hoffman EJ, Andreaco M, and Williams CW. A comparison of PET detector modules employing rectangular and round photomultipler tubes. IEEE Transactions on Nuclear Science 1995 42:1064–1068.

Cloquet C, Sureau FC, Defrise M, Simaeys GV, Trotta N, and Goldman S. Non-Gaussian space-variant resolution modeling for list-mode reconstruction. Physics in Medicine and Biology 2010 55:5045–5066.

Conti M. Why is TOF PET reconstruction a more robust method in the presence of inconsistent data? Physics in Medicine and Biology 2011 56:155–168.

Defrise M, Panin V, Michel C, and Casey ME. Continuous and discrete data rebinning in Time-of-Flight PET. IEEE Transactions on Medical Imaging 2008 27:1310–1322.

El Fakhri G, Surti S, Trott CM, Scheuermann J, and Karp JS. Improvement in lesion detection with whole-body oncologic time-of-flight PET. Journal of Nuclear Medicine 2011 52:347–353.

Hu Z, Wang W, Gualtieri EE, Hsieh YL, Karp JS, Matej S, Parma MJ, Tung CH, Walsh ES, Werner M, and Gagnon D. An LOR-based fully-3D PET image reconstruction using a blob-basis function. IEEE Medical Imaging Conference 2007 (paper M26–228).

Kadrmas DJ. LOR-OSEM: statistical PET reconstruction from raw line-of-response histograms. Physics in Medicine and Biology 2004 49:4731–4744.

Kadrmas DJ, Casey ME, Black NF, Hamill JJ, Panin VY, and Conti M. Experimental comparison of lesion detectability for four fully-3D PET reconstruction schemes. IEEE Transactions on Medical Imaging 2009 28:523–534.

Karp JS, Surti S, Daube-Witherspoon ME, Freifelder R, Cardi CA, Adam LE, Bilger K, and Muehllehner G. Performance of a brain PET camera based on Anger-logic gadolinium oxyorthosilicate detectors. Journal of Nuclear Medicine 2003 44:1340–1349.

Karp JS, Surti S, Daube-Witherspoon ME, and Muehhlehner G. The benefit of time-of-flight in PET imaging: experimental and clinical results. Journal of Nuclear Medicine 2008 49:462–470.

Kuhn A, Surti S, Karp JS, Raby PS, Shah KS, Perkins AE, and Muehllehner G. Design of a lanthanum bromide detector for time-of-flight PET. IEEE Transactions on Nuclear Science 2004 51:2550–2557.

Liu X, Comtat C, Michel C, Kinahan P, Defrise M, and Townsend D. Comparison of 3-D reconstruction with 3D-OSEM, and with FORE + OSEM for PET. IEEE Transactions on Medical Imaging 2001 20:804–814.

Lucy LB. An iterative technique for the rectification of observed images. Astronomical Journal 1974 79:745–754.

Matej S and Browne JA. Performance of a fast maximum likelihood algorithm for fully 3D PET reconstruction. Three-dimensional image reconstruction in radiology and nuclear medicine. P Grangeat and JL Amans, eds. Kluwer Academic Publishers. 1996 297–316.

Matej S and Lewitt M. Practical considerations for 3D image reconstruction using spherically symmetric volume elements. IEEE Transactions on Medical Imaging 1996 15:68–78.

Perkins AE, Saffer JR, Scheuermann JS, Werner ME, Karp JS, and Divgi CR. Clinical optimization of the acquisition time of FDG time-of-flight PET. Journal of Nuclear Medicine 2007, Abstract Book Supplement 48:91P.

Perkins AE, Daube-Witherspoon ME, Surti S, Clementel E, and Karp JS. Reduction in variability of clinical lesion quantification with TOF-PET imaging. 2010 IEEE Medical Imaging Conference (paper M20-3) 2010.

Popescu LM, Matej S, and Lewitt RM. Iterative image reconstruction using geometrically ordered subsets with list-mode data. IEEE Medical Imaging Conference (paper M9-211) 2004.

Richardson WH. Bayesian-based iterative method of image restoration. Journal of the Optical Society of America 1972 62:55–59.

Snyder DL and Miller MI. The use of sieves to stabilize images produced with the EM algorithm for emission tomography. IEEE Transactions on Nuclear Science 1985 NS-32:3864–3872.

Strandberg K and Djoury MA. Philips delivers breakthrough performance with Astonish TF reconstruction technology. Philips Astonish TF White Paper 2011.

Surti S, Karp JS, Freifelder R, and Liu F. Optimizing the performance of a PET detector using discrete GSO crystals on a continuous lightguide. IEEE Transactions on Nuclear Science 2000 47:1030–1036.

Surti S, Kuhn A, Werner ME, Perkins AE, Kolthammer J, and Karp JS. Performance of Philips Gemini TF PET/CT scanner with special consideration for its Time-of-Flight imaging capabilities. Journal of Nuclear Medicine March 2007 48:471–480.

Surti S and Karp JS. Experimental evaluation of a simple lesion detection task with time-of-flight PET. Physics in Medicine and Biology 2009 54:373–384.

Surti S, Scheuermann J, El Fakhri G, Daube-Witherspoone ME, Lim R, Abi-Hatem N, Moussallem E, Bernard F, Mankoff D, and Karp JS. Impact of Time-of-Flight PET on whole-body oncologic studies: a human observer lesion detection and localization study. Journal of Nuclear Medicine 2011 52:712–719.

Tipnis S, Hu Z, Gagnon D, and O'Donnell JK. Time-of-flight PET for Rb-82 cardiac perfusion imaging. Journal of Nuclear Medicine 2008 Abstract Book Supplement 49:74P.

Tomatani T. Image-reconstruction and noise evaluation in photon time-of-flight assisted positron emission tomography. IEEE Transactions on Nuclear Science 1981 28:4582–4589.

Vandenberghe S, Daube-Witherspoon ME, Lewitt RM, and Karp JS. Fast reconstruction of 3D time-of-flight PET data by axial rebinning and transverse mashing. Physics in Medicine and Biology 2006 51:1603–1621.

Wang W, Hu Z, Gualtieri EE, Parma MJ, Walsh ES, Sebok D, Hsieh YL, Tung CH, Song X, Griesmer JJ, Kolthammer JA, Popescu LM, Werner M, Karp JS, and Gagnon D. Systematic and Distributed Time-of-Flight Listmode PET Reconstruction. IEEE Medical Imaging Conference (paper M04-2) 2006.

Watson CC. Extension of single scatter simulation to scatter correction of time-of-flight PET. IEEE Transactions on Nuclear Science 2007 54:1679–1686.

Werner ME, Surti S, and Karp JS. Implementation and evaluation of a 3D PET single scatter simulation with TOF modeling. IEEE Medical Imaging Conference (paper M05-3) 2006.

Wong W, Uribe J, Hicks K, and Hu G. An analog decoding BGO block detector using circular photomultipliers. IEEE Transactions on Nuclear Science 1995 42:1095–1101.

Philips Healthcare is part of Royal Philips Electronics

How to reach us
www.philips.com/healthcare
healthcare@philips.com

Asia
+49 7031 463 2254

Europe, Middle East, Africa
+49 7031 463 2254

Latin America
+55 11 2125 0744

North America
+1 425 487 7000
800 285 5585 (toll free, US only)

Please visit www.philips.com/AstonishTF

Printed in The Netherlands.
4522 962 74041 * JUN 2011